






Research Article

A Two-Stage Cooperative Adaptive Cruise Control for Connected Automated Vehicles in Multislope Roads considering Communication Delay and Actuator Delay

Jianjie Kuang ¹, Gangfeng Tan ^{1,2}, Xuexun Guo ^{1,2}, Xiaofei Pei ^{1,2}
and Dengzhi Peng ^{1,3}

¹School of Automotive Engineering, Wuhan University of Technology, Wuhan 430070, China

²Hubei Key Laboratory of Advanced Technology for Automotive Components, Wuhan University of Technology, Wuhan 430070, China

³Dongfeng Off-road Vehicle Co. Ltd, Shiyan 442013, China

Correspondence should be addressed to Gangfeng Tan; auto_nova@whut.edu.cn

Received 28 April 2023; Revised 4 August 2023; Accepted 16 January 2024; Published 30 January 2024

Academic Editor: Francesco Galante

Copyright © 2024 Jianjie Kuang et al. This is an open access article distributed under the Creative Commons Attribution License, which permits unrestricted use, distribution, and reproduction in any medium, provided the original work is properly cited.

Connected and automated vehicle platoons (CAVPs) are considered an effective way to alleviate traffic congestion, reduce the incidence of traffic accidents, and improve vehicle economy in the intelligent transportation system (ITS). Vehicles in the CAVPs can communicate with each other through V2X technology, which could optimize the economy of the platoon. Cooperative adaptive cruise control (CACC) can make effective use of the characteristics of CAVPs and contribute to resource conservation, ecological driving, and traffic system development. In this paper, a two-stage CACC method is proposed for CAVPs to reduce fuel consumption in the multislope road section. In the first stage, the optimal velocity profiles for the leader based on dynamic programming (DP) are planned according to the road information and the fuel consumption model. In the second stage, a vehicle longitudinal third-order differential dynamics model is utilized to build the platoon time-delay system considering communication delay and actuator delay. A feedback controller is developed for each vehicle considering the internal stability and the string stability of the CAVPs. Results show that the proposed method can save 5.33% of fuel consumption compared to the constant speed cooperative adaptive cruise control (CS-CACC) method and has a better tracking performance compared to the model predictive control (MPC) method. The CACC method proposed in this paper can provide a theoretical basis and data support for building an ecological CACC strategy for CAVPs.

1. Introduction

The rapid development of automobiles has brought convenience to people's mobility, but the increase in the total number of automobiles has also increased traffic congestion, the probability of traffic accidents, and the rate of global consumption of nonrenewable energy. Therefore, more and more researchers are focusing on the fields of connected and automated vehicles (CAVs) and intelligent transportation systems (ITSs) to mitigate the effects of the above problems [1]. Among them, cooperative adaptive cruise control (CACC) is considered a method that can effectively increase the capacity of the traffic flow and reduce energy

consumption [2]. CACC is mainly used in platoons that could contain different power source types and different intelligent levels of vehicles [3]. Each vehicle in the platoon could obtain other vehicles' information through a variety of sensors and network communication technologies. Platoons using CACC could reduce the probability of accidents and energy consumption, improve the capacity of the traffic flow, and achieve optimal driving objectives [4]. Therefore, more and more researchers have begun to study CACC technology and use it in a variety of scenarios to achieve the desired goals.

CACC is capable of functioning in a variety of scenarios. In the mixed traffic flow scenarios, platoons consisting of both CAVs and human-driving vehicles could significantly

increase the capacity of the traffic flow and reduce energy consumption by using CACC. The proportion of CAVs in a platoon could also significantly affect the fuel consumption and the average speed of the platoon [5, 6]. As for the traffic flow, the appropriate penetration and size of platoons could increase the capacity of the traffic and reduce the risk of potential traffic accidents due to the unreasonable lane-changing behaviors of other environmental vehicles [7]. However, the stability, safety, and economy of the whole traffic flow will also be reduced as the size of platoons increases [8]. In the traffic intersection scenarios, the application of CACC can enable platoons to efficiently pass through intersections and reduce the energy consumption of platoons while avoiding traffic congestion. In the traffic intersections with uncertain signal timing, the authors in [9] proposed a data-driven chance-constrained eco-driving control approach based on using dynamic programming (DP) to solve the optimal problem, which is verified to have high robustness and fuel economy. The authors in [10] proposed an eco-driving approach for CAVs stopped and CAVs moved at traffic intersections. The purpose is to allow CAVs in different driving states to pass through the traffic intersections with the fastest speed and the least energy consumption without congestion. For long-size platoons, the authors in [11] proposed an ECU-CACC that divides the platoon into several mini-ECU which is a platoon but has a smaller size to pass through the traffic intersection efficiently and economically. CACC can also be used for cooperative control of platoons and traffic intersection infrastructures [12]. The signaling infrastructure incorporating CACC can assign signal priority to the intersection based on the driving status of platoons that are about to pass through the intersection, thus allowing platoons to pass through the intersection with minimal fuel consumption. In the scenarios of platoons merging and joining, the application of CACC could effectively avoid collisions within the platoon and select the appropriate timing [13] to realize platoon merging and joining, thus improving the capacity of the traffic flow and reducing the energy consumption [14]. CACC is mainly used for the longitudinal control of platoons in this type of scenario [15], which allows the platoon to leave enough spacing to allow other vehicles to join. Also, a decision-making system for insertion position and insertion timing according to traffic environments is crucial [16]. Another important CACC application scenario is the platoon cruising scenario. In this scenario, the main CAVs of the platoon are commercial vehicles for logistics transportation. The platoon usually needs to keep a fixed formation for traveling on roads with different slopes. The application of CACC could enable the platoon to cruise according to the optimal energy consumption and realize eco-driving [17, 18]. In this paper, the main research scenario focuses on the platoon cruising scenario.

To be able to achieve optimal energy consumption driving in platoon cruising scenarios, many approaches have been proposed. One type of the abovementioned approaches is to use real-time optimization to achieve platoon control with optimal energy consumption objectives by using the fuel

consumption of the vehicles as a part of a cost function. Tracking error, comfort, and energy consumption could be considered as objectives using different weights to build cost function [19]. A real-time CACC optimization method considering input delay is proposed based on model predictive control (MPC) using energy consumption and band-stop function as the cost functions [20]. Meanwhile, the actuator delays are considered further in subsequent work [21]. In the literature [22], a real-time data-driven CACC optimization method based on DP for unknown dynamic heterogeneous vehicle platoons is proposed. Although the real-time optimization approach can fully incorporate the current driving state of platoons to make the optimal control inputs, however, real-time optimization requires a large amount of computation, which is a considerable challenge for the hardware on the vehicle. Therefore, although real-time optimization can ensure that platoons' control is always optimized, it also needs higher-performance hardware. If the planning layer and control layer in the CACC are separated, combining multiple control steps of platoons to optimize together can reduce the computation quantity of real-time optimization while achieving the optimal goal of platoon cruising [23]. A two-layer structure of CACC is proposed in the literature [24]. The upper layer adopts a centralized ecological speed planning (CESP) algorithm based on DP to produce optimal speed profiles, and the lower layer designs a distributed collision-free speed tracking (DCST) control method to make the platoon follow the optimal speed profiles without collision. The same idea is also found in the literature [25, 26]. In literature [27], a three-layer eco-CACC optimal control structure is proposed, which considers the characteristics of the motor and optimizes them.

A hierarchical CACC could reduce the computation quantity of vehicle hardware while ensuring optimization results. However, when considering CACC for platoon cruising, there are still many factors that need to be considered which will affect the effectiveness of CACC. These factors include the vehicle dynamics model, road conditions, communication topology, communication delay, and actuator state [4, 28–30]. The vehicle dynamics model is the model basis for realizing the goal of optimal energy consumption of platoon cruising [31]. The vehicle's longitudinal second-order [32] and third-order [33] dynamic models are used frequently, whereas the third-order dynamic model includes modeling of actuator delays. For the vehicle's power source, due to the characteristics of the engine, the engine energy consumption model is generally fitted by empirical data, such as the transient polynomial fuel consumption model (TPFM) [34]. In the literature [35], empirical formulas for fuel consumption modeling of heavy-duty vehicles are established by analyzing experimental data. Rolling resistance coefficient [36] and air resistance coefficient [25, 37] will also affect the fuel consumption of platoons. For communication topology, they could classically be categorized into six types [38]: (1) predecessor-following (PF) topology; (2) bidirectional (BD) topology; (3) predecessor-leader-following (PLF) topology; (4) two-predecessor-following (TPF) topology; (5) bidirectional-leader-following (BDLF) topology; and (6) two-predecessor-leader-following (TPLF) topology. The abovementioned six communication topologies are studied in the

literature [39]. The platoon tends to be more stable as more information is received by the vehicles, but BD will increase the risk of tailgating. In literature [40], it was found that PLF is better than PF and LF. And PF has the worst platoon stability performance among these three topologies. The communication delay and actuator state also affect the effectiveness of CACC and platoons' stability [41]. Designing a feedback controller for a platoon based on a time-delay system could keep the platoons stable [42, 43] by considering the communication delay and actuator delay as constants or predicting them [44]. The authors in [45] investigated the effects of actuator faults and saturation on platoons and proposed an adaptive fault-tolerant control method based on nonlinear vehicle dynamics and a new quadratic spacing policy to ensure individual vehicle stability, string stability, and traffic flow stability. When communication fails, literature [46, 47] used onboard sensors to obtain information from other vehicles. In [48], historical data are used to predict the traveling status of other vehicles based on the long short-term memory (LSTM) neural network.

In summary, in the platoon cruising scenarios, CACC could take full advantage of platoons and can reduce the energy consumption of platoons. Therefore, many CACC optimization strategies have been proposed, including real-time optimization and hierarchical optimization. Meanwhile, lots of factors that may affect the effectiveness of CACC have been studied. These works have been of great help to future generations in continuing to study CACC for platoon cruising. However, in the current research, very few of them have integrated communication delay, actuator delay, and feedback controller design based on communication topology in a hierarchical CACC. This paper expects to fill the gap in this section. In this paper, a two-stage CACC for platoon cruising is proposed to achieve the optimal energy consumption goal by integrating communication delay, actuator delay, and communication topology. The first stage is the offline stage. After determining the start location and the destination, the global optimal velocity profiles are planned for the leader using DP based on the longitudinal third-order dynamic model and fuel energy consumption model. The second stage is the online stage, which builds a feedback controller for each vehicle to follow the optimal velocity profiles and target spacing based on the communication topology and the stability condition considering the communication delay and actuator delay. Compared with the previous work, the main contributions of this paper are as follows: (1) based on the PLF topology, the communication delay and actuator delay of vehicles are comprehensively considered to construct the feedback controller of each vehicle, which ensures the internal stability and string stability during platoon cruising, and (2) it combines the advantages of a hierarchical CACC and the improvement of the effectiveness of CACC by considering the communication delay and actuator delay to provide the theoretical basis and data support for the improvement of CACC for platoon cruising.

The rest of this paper is organized as follows. Section 2 covers the entire paper's structure, as well as the longitudinal dynamic model of the vehicle and the energy consumption

model. Section 3 describes the DP algorithm's process for global optimal velocity profiles; Section 4 provides a feedback controller based on three-order differential vehicle dynamics models and sets boundary constraints for controller parameters, considering the internal stability and string stability. Section 5 discusses simulation results, and Section 6 gives conclusions.

2. System Description

2.1. Platoon Communication Topology. According to the papers [38–41], it is mentioned that platoons could better maintain stability with more vehicle information taken into consideration, and the bidirectional topology would increase rear-end collision risk. Considering the platoon stability and the amount of data that need to be processed, the predecessor-leader following topology is used in this paper and is shown in Figure 1.

In this paper, a two-stage CACC control strategy is used, and in the first stage, the vehicle longitudinal dynamics model and the engine energy consumption model are considered to design the platoon energy cost function. Then, the global optimal velocity profiles of the leader are planned by combining the road slope data and the DP algorithm. The leader will follow the global optimal velocity profiles throughout the whole course. In the second stage, a vehicle longitudinal third-order differential dynamics model is used to build the platoon time-delay system considering vehicle actuator delays and communication delays. A feedback controller based on an error model is constructed for each vehicle, and the feedback gain parameters of the controller are deduced based on the internal stability and the string stability. Each following vehicle uses its feedback controller to follow the leader and the predecessor by acquiring the speed information and coordinating information of the leader and the predecessor. By the abovementioned two-stage method, the platoon eventually achieves stable tracking for the target spacing and optimal velocity profiles. The overall structure flowchart of the full paper is shown in Figure 2.

2.2. Vehicle Dynamics. The vehicle dynamics model is the basis of the control strategy construction. In the construction of the CACC control strategy, the second-order longitudinal dynamics model of the vehicle or the third-order longitudinal dynamics model is typically considered [32, 33], where the third-order dynamics model accounts for the delay of the vehicle actuator. Therefore, the third-order vehicle longitudinal dynamics model is utilized in this paper which is represented as follows:

$$\begin{cases} \dot{p}_i(t) = v_i(t), \\ \dot{v}_i(t) = a_i(t), \\ \dot{a}_i(t) = -\frac{1}{\eta}a_i(t) + \frac{1}{\eta}u_i(t), \end{cases} \quad (1)$$

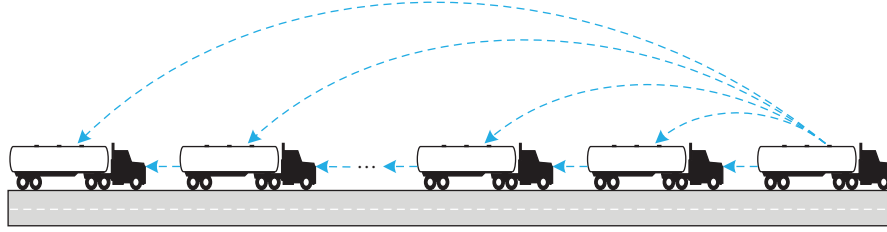


FIGURE 1: The predecessor-leader-following topology.

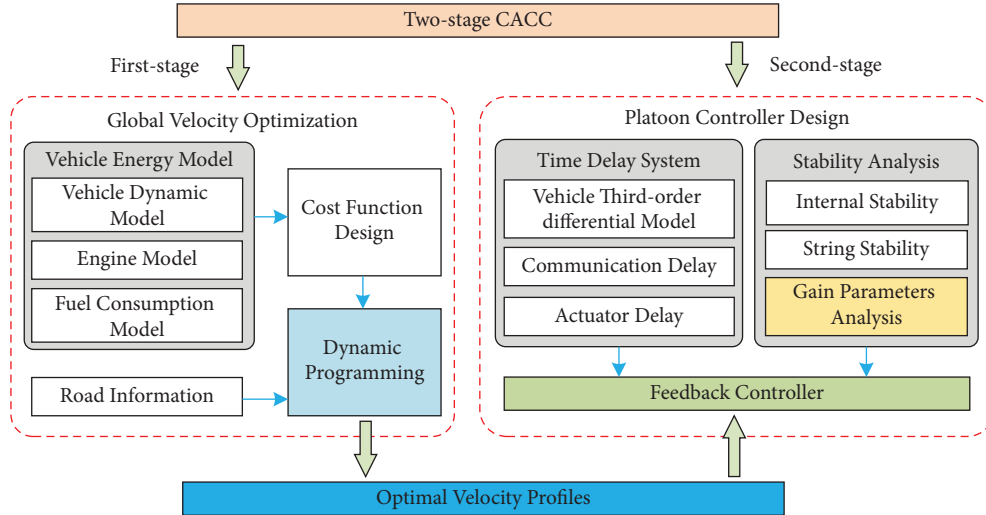


FIGURE 2: The overall structure flowchart of the two-stage CACC strategy.

where $p_i(t)$ denotes the longitudinal coordinate of the i th vehicle, $v_i(t)$ denotes the longitudinal velocity of the i th vehicle, $a_i(t)$ denotes the longitudinal acceleration of the i th vehicle, η denotes the actuator delay, and $u_i(t)$ denotes the control input of the i th vehicle.

According to the vehicle's driving force resistance balance equation and Newton's second theorem, the following relationship exists between the vehicle's longitudinal driving force and the vehicle's input:

$$m_i u_i(t) = \frac{T_i(t)}{r_i} - \frac{C_{di} A_{wi} \rho_a v_i^2(t)}{2} - m_i g f_i \cos(\theta(p_i(t))) - m_i g \sin(\theta(p_i(t))) - \delta m_i a_i(t), \quad (2)$$

where m_i denotes the mass of the i th vehicle, $T_i(t)$ denotes the driving torque of the i th vehicle, r_i denotes the radius of the vehicle tires of the i th vehicle, A_{wi} denotes the windward area of the i th vehicle, C_{di} denotes the air drag coefficient of the i th vehicle, ρ_a denotes the density of air, g denotes the acceleration of gravity, f_i denotes the rolling resistance coefficient of the i th vehicle, $\theta(p_i(t))$ denotes the slope of the road at the position $p_i(t)$, and δ denotes the mass rotation coefficient of the i th vehicle.

The rolling resistance coefficient of the vehicle is calculated according to the empirical formula for heavy vehicles from [36], as follows:

$$f_i = 0.0076 + 0.0002016v_i(t). \quad (3)$$

$d_i(t)$ is used to express the distance between the i th vehicle and the predecessor. The calculated formula is as follows:

$$d_i(t) = p_{i-1}(t) - p_i(t), \quad (4)$$

where $p_{i-1}(t)$ denotes the position of the $(i-1)$ th vehicle and $p_i(t)$ denotes the position of the i th vehicle.

By controlling the spacing between vehicles in a platoon, the air drag coefficient can be reduced, thereby effectively reducing the energy consumption of the vehicles [37]. In this paper, the air drag coefficient of the vehicle at different spacing is calculated by using the methods described in the literature [20, 25]. The calculation is shown as follows:

$$C_{di} = \begin{cases} C_d, & i = 1, \\ C_d \left(1 - \frac{c_1}{c_2 + d_i(t)} \right), & i = 2, \dots, n, \end{cases} \quad (5)$$

where C_d denotes the normal air drag coefficient of the vehicle and c_1 and c_2 are the constants based on experimental data.

3. Optimal Velocity Sequence Planning

3.1. Fuel Consumption Model. The fuel consumption model of a vehicle is influenced by various factors, such as engine type, air resistance, road class, body mass, and tire size [35]. The complexity of the engine fuel consumption model is further compounded by the impact of transmission gear ratios and clutches on fuel consumption. In this paper, the engine fuel consumption model is simplified. It is assumed that the engine model employed is a CVT engine with the vehicle's transmission gear ratio always maintained at its optimal value. In addition, the clutch of the vehicle is assumed to be engaged, and its effect is disregarded. The engine fuel consumption model used in this paper is based on the fitted mathematical model described in [25], which is as follows:

$$Q_i(t) = \begin{cases} \gamma_0 + \gamma_1 P_{ei}(t) + \gamma_2 P_{ei}^2(t) P(t) \geq 0, \\ \gamma_0 P(t) < 0, \end{cases} \quad (6)$$

where $Q_i(t)$ denotes the fuel consumption rate of the i th vehicle, $P_{ei}(t)$ denotes the engine output power of the i th vehicle, and γ_0 , γ_1 , and γ_2 are constants fitted to the experimental data.

Considering the powertrain of the vehicle, the formula for calculating the output power of the engine is as follows:

$$P_{ei}(t) = \frac{T_{ei}(t)n_{ei}(t)}{9550}, \quad (7)$$

where $T_{ei}(t)$ denotes the output torque of the engine and $n_{ei}(t)$ denotes the speed of the engine, which are calculated by using the following equations:

$$\begin{cases} T_{ei}(t) = \frac{T_i(t)}{i_g i_0 \xi}, \\ n_{ei}(t) = \frac{3.6v_i(t)i_g i_0}{0.377r_i}, \end{cases} \quad (8)$$

where i_g denotes the transmission gear ratio, i_0 denotes the final reduction drive ratio, and ξ represents the mechanical efficiency of the transmission system. By combining equations (2), (7), and (8), the output power of the engine can be expressed in the following form:

$$P_{ei}(t) = \frac{3.6v_i(t)T_i(t)}{0.377 \times 9550r_i \xi} \quad (9)$$

The abovementioned equation is the mathematical expression of the fuel consumption model used in this paper.

3.2. DP Algorithm Structure. In this paper, a dynamic programming (DP) algorithm is employed to determine the optimal velocity profiles for the leader in the first stage. DP divides the entire problem into subproblems and obtains the global optimization result by solving the optimization results of these subproblems. According to Bellman's optimization strategy, the remaining inputs and states of the entire system will converge to the optimal state and steps regardless of the initial state and the initial inputs [24]. The task of finding the optimal velocity for the leader vehicle can be reformulated as an optimal problem that can be solved by using the classical DP algorithm through the discretization of road nodes and speed nodes. By searching for the minimal fuel consumption velocity profiles from the original position to the end position within one subproblem, the overall optimal velocity profiles could be calculated after solving all subproblems. The principle schematic of the DP is shown in Figure 3.

In this paper, it is assumed that the longitudinal position of the vehicle is discretized from the starting point to the ending point as $P = [p(1), p(2), \dots, p(k), \dots, p(n)]$. The distance between each position point is Δs , and this distance is fixed. $p(1)$ is the starting point, and the discrete longitudinal points satisfy the following relationship:

$$p(i) - p(i-1) = \Delta s, \quad i = 1, 2, \dots, n. \quad (10)$$

The same discretization method is applied to the velocity, which is discretized into the following form: $V = [v(1), v(2), \dots, v(k), \dots, v(m)]$. The velocity interval is Δv .

The core equation of dynamic programming is represented as follows:

$$\begin{cases} J[v(k), v(l), p(k)] = L[S(v(k), p(k)), S(v(l), p(k+1))] + J_{\min}[v(l), p(k+1)], \\ J_{\min}[v(k), p(k)] = \min\{J[v(k), v(j), p(k)], \quad j = 1, 2, \dots, n\}, \end{cases} \quad (11)$$

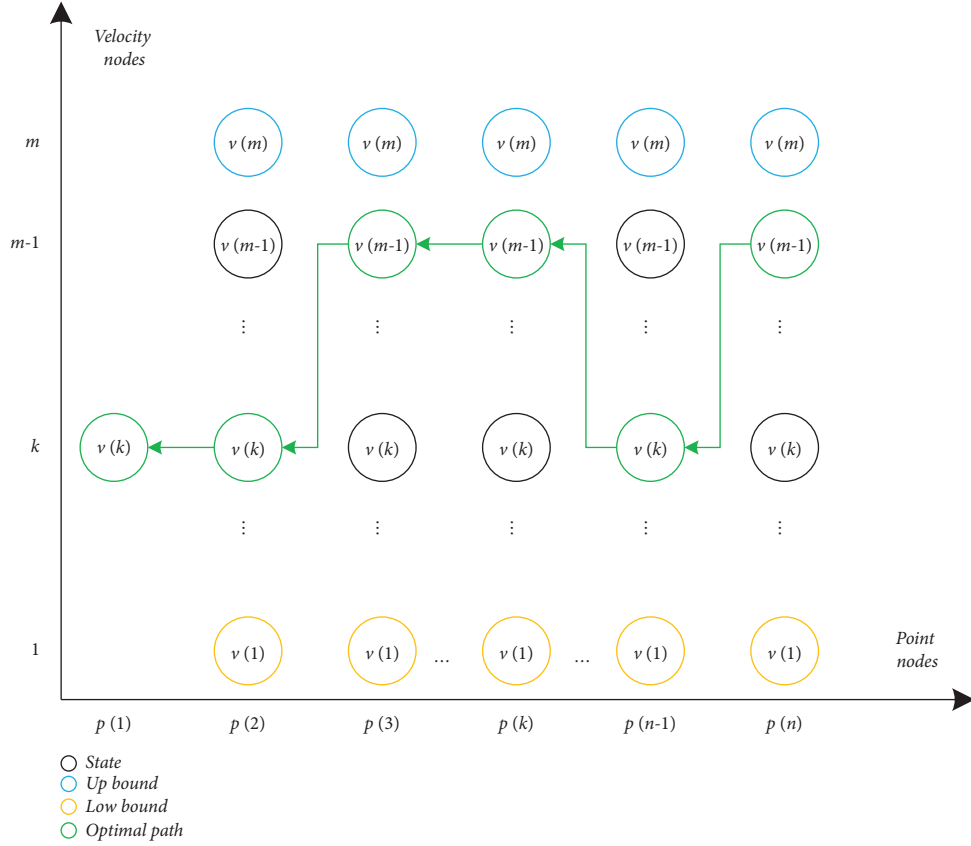


FIGURE 3: The principle schematic of the DP algorithm.

where $J[v(k), v(l), p(k)]$ represents the total cost from the state point $J[v(k), v(l), p(k)]$ to the endpoint and the next state point is $S(v(l), p(k+1))$, where $L[S(v(k), p(k)), S(v(l), p(k+1))]$ represents the cost from the state point $S(v(k), p(k))$ to the next state point $S(v(l), p(k+1))$ and $J_{\min}[v(k), p(k)]$ represents the global minimum cost from the state point $S(v(k), p(k))$ to the endpoint. $L[S(v(k), p(k)), S(v(l), p(k+1))]$ is calculated by using the following equation:

$$L = \sum_{i=1}^N \int_{t_s}^{t_e} Q_i(t) dt, \quad (12)$$

where t_s denotes the time when the leader arrives at the state point $S(v(k), p(k))$ and t_e denotes the time when the leader vehicle arrives at the state point $S(v(l), p(k+1))$.

In this paper, it is assumed that the following vehicles keep the same speed as the leader and adhere to the preset spacing. Consequently, both the following vehicles and the leader will complete their travel simultaneously. The key distinguishing factors are the differing positions of the following vehicles and the leader, as well as the variation in slope along the road section. The planning process for the leader vehicle's optimal velocity profiles in this study is based on minimizing the overall energy consumption of the entire platoon.

After establishing the abovementioned model of the optimal velocity sequence and the cost function, the optimal velocity sequence for the leader could be calculated by using the DP, which is shown in Table 1, to solve the above mentioned optimal question.

4. Platoon Control Model

4.1. Error Model. The spacing in a platoon is generally divided into two strategies: constant spacing (CS) strategy and constant time heading (CTH) strategy [21]. In this paper, the CS strategy is employed. Under the CS strategy, the target longitudinal position of the current vehicle is determined based on the position of the leader vehicle and is calculated as follows:

$$p_{i,d}(t) = p_1(t) - (i-1)d_0, \quad (13)$$

where $p_{i,d}(t)$ denotes the target position of the i th vehicle, $p_1(t)$ denotes the position of the leader, and d_0 denotes the preset spacing. Then, the error of the longitudinal position of the i th vehicle can be calculated by using the following equation:

$$\tilde{p}_i(t) = p_1(t) - (i-1)d_0 - p_i(t). \quad (14)$$

The error of the spacing between the current vehicle and the previous vehicle can be expressed as follows:

TABLE 1: The DP optimal velocities algorithm.

Algorithm 1: DP optimal velocities algorithm

Input: $P = [P(1), P(2), \dots, P(n)]$, $v = [P(1), P(2), \dots, P(m)]$, Δs , v_{ini} , a_{min} , a_{max}

Output: V_{best}

- (1) *Initiation* $J_{map} = \text{zeros}(n, m)$
- (2) **for** $i = n - 1$: 1: 1 **do**
- (3) **for** $j = 1$: 1: m **do**
- (4) *Initiation* $J_v = \text{zeros}(1, m)$
- (5) **for** $k = 1$: 1: m **do**
- (6) calculate duration time Δt from $S(v(j), P(i))$ to $S(v(k), P(i + 1))$
- (7) calculate acceleration a from $v(j)$ to $v(k)$
- (8) **if** $a \in [a_{min}, a_{max}]$ **then**
- (9) calculate $L[S(v(j), P(i)), S(v(k), P(i + 1))]$
- (10) **else**
- (11) set $L[S(v(j), P(i)), S(v(k), P(i + 1))] = \text{inf}$
- (12) **end if**
- (13) $J_v(1, k) = L[S(v(j), P(i)), S(v(k), P(i + 1))] + J_{map}(i + 1, k)$
- (14) **end for**
- (15) $J_{map}(i, j) = \min \{J_v\}$
- (16) **end for**
- (17) **end for**
- (18) find V_{best} from J_{map}
- (19) **return** V_{best}

$$\tilde{p}_{i,i-1}(t) = p_{i-1}(t) - d_0 - p_i(t) = \tilde{p}_i(t) - \tilde{p}_{i-1}(t). \quad (15)$$

The abovementioned equation represents the spacing error, and in the next section, we will design the feedback controller of the vehicle based on the aforementioned error model.

4.2. Control System Design. In this paper, the communication topology of the platoon adopts the predecessor-leader following topology. The current vehicle receives driving information from both the leader and the predecessor,

necessitating the examination of spacing errors with both. Accordingly, the design principles for a linear feedback controller in this scenario are as follows:

$$u_i(t) = k_1(\tilde{p}_i(t) + \dot{\tilde{p}}_i(t)) + k_2(\tilde{p}_i(t) - \tilde{p}_{i-1}(t) + \dot{\tilde{p}}_i(t) - \dot{\tilde{p}}_{i-1}(t)). \quad (16)$$

Considering the communication delay within the platoon, the current vehicle input is rewritten in the following form:

$$u_i(t) = k_1(\tilde{p}_i(t - \tau(t)) + \dot{\tilde{p}}_i(t - \tau(t))) + k_2(\tilde{p}_i(t - \tau(t)) - \tilde{p}_{i-1}(t - \tau(t)) + \dot{\tilde{p}}_i(t - \tau(t)) - \dot{\tilde{p}}_{i-1}(t - \tau(t))) \\ = (k_1 + k_2)(\tilde{p}_i(t - \tau(t)) + \dot{\tilde{p}}_i(t - \tau(t))) - k_2(\tilde{p}_{i-1}(t - \tau(t)) + \dot{\tilde{p}}_{i-1}(t - \tau(t))), \quad (17)$$

where $\tau(t)$ represents the communication delay time. The entire system is set up as a slow delay system, where the following conditions should be met:

$$\begin{cases} 0 \leq \tau(t) \leq h, \\ \dot{\tau}(t) \leq \varphi. \end{cases} \quad (18)$$

Since the leader is the first vehicle in the platoon and does not have a predecessor, the controller of the leader vehicle is designed in the following form:

$$u_1(t) = (k_1 + k_2)(\tilde{p}_1(t - \tau(t)) + \dot{\tilde{p}}_1(t - \tau(t))), \quad (19)$$

where $\tilde{p}_1(t)$ represents the error between the actual position of the leader vehicle and the target position and $\dot{\tilde{p}}_1(t)$ represents the error between the velocity of the leader and the target velocity. In this paper, the target velocity is the optimal vehicle velocity at the current position of the leader vehicle calculated according to Section 3. Therefore, in this paper, $\tilde{p}_1(t) \triangleq 0$.

Based on the error model and the input equation, the following differential dynamics equation can be obtained:

$$\begin{cases} \dot{\tilde{p}}_i(t) = v_1(t) - v_i(t), \\ \ddot{\tilde{p}}_i(t) = a_1(t) - a_i(t), \\ \ddot{\tilde{p}}_{i-1}(t) = \dot{a}_1(t) - \dot{a}_i(t). \end{cases} \quad (20)$$

$$\begin{aligned} \ddot{\tilde{p}}_{i-1}(t) = & -\frac{1}{\eta}\ddot{\tilde{p}}_i(t) + \frac{1}{\eta}[(k_1 + k_2)(\tilde{p}_1(t - \tau(t)) + \dot{\tilde{p}}_1(t - \tau(t))) - (k_1 + k_2)(\tilde{p}_i(t - \tau(t)) + \dot{\tilde{p}}_i(t - \tau(t))) \\ & + k_2(\tilde{p}_{i-1}(t - \tau(t)) + \dot{\tilde{p}}_{i-1}(t - \tau(t)))] \end{aligned} \quad (21)$$

Let $x_i(t) = [\tilde{p}_i, \dot{\tilde{p}}_i, \ddot{\tilde{p}}_i(t)]^T$, then according to equations (17), (19), (20), and (21), the following equations exist:

$$\begin{aligned} x_i(t) = & A_i x_i(t) + B_1 x_1(t - \tau(t)) - B_1 x_i(t - \tau(t)) \\ & + B_2 x_{i-1}(t - \tau(t)), \end{aligned} \quad (22)$$

where

$$\begin{aligned} A_i = & \begin{bmatrix} 0 & 1 & 0 \\ 0 & 0 & 1 \\ 0 & 0 & -\frac{1}{\eta} \end{bmatrix}, \\ B_1 = & \begin{bmatrix} 0 & 0 & 0 \\ 0 & 0 & 0 \\ \frac{k_1 + k_2}{\eta} & \frac{k_1 + k_2}{\eta} & 0 \end{bmatrix}, \\ B_2 = & \begin{bmatrix} 0 & 0 & 0 \\ 0 & 0 & 0 \\ \frac{k_2}{\eta} & \frac{k_2}{\eta} & 0 \end{bmatrix}. \end{aligned} \quad (23)$$

Let $x(t) = [x_1(t), x_2(t), \dots, x_n(t)]^T$, then the whole platoon system could be rewritten as

$$\dot{x}(t) = Ax(t) + Bx(t - \tau(t)), \quad (24)$$

where

Bringing $u_i(t)$ into the differential dynamic equation, the abovementioned $\tilde{p}_i(t)$ could be rewritten as

$$\begin{cases} A = \text{diag}\{A_1, A_2, \dots, A_n\}, \\ B = \begin{bmatrix} B_1 & 0_{3 \times 3} & 0_{3 \times 3} & 0_{3 \times 3} & \dots & 0_{3 \times 3} \\ B_1 + B_2 & -B_1 & 0_{3 \times 3} & 0_{3 \times 3} & \dots & 0_{3 \times 3} \\ B_1 & B_2 & B_1 & 0_{3 \times 3} & \dots & 0_{3 \times 3} \\ \vdots & \vdots & \vdots & \ddots & \ddots & \vdots \\ B_1 & 0_{3 \times 3} & \dots & B_2 & -B_1 & 0_{3 \times 3} \\ B_1 & 0_{3 \times 3} & \dots & 0_{3 \times 3} & B_2 & -B_1 \end{bmatrix}. \end{cases} \quad (25)$$

In this section, we convert the entire system into a standardized model of a time-delay system. The subsequent section will delve into the analysis and explanation of the system's stability.

4.3. Internal Stability Analysis. According to the Lyapunov–Krasovskii generalized equation for the aboveproposed system, there exist matrices $(P, Q, S, R, P_2, P_3) \in \mathbb{R}^{3n \times 3n}$. P, Q, S, R are positive definite matrices. P_2 and P_3 are matrices of proper dimension, and the whole system is asymptotically stable when the following matrix inequality has a solution [37]:

$$\begin{cases} \begin{bmatrix} \Phi_{11} & \Phi_{12} & 0 & P_2^T B + R \\ * & \Phi_{22} & 0 & P_3^T B \\ * & * & -S + R & R \\ * & * & * & -(1 - \varphi)Q - 2R \end{bmatrix} < 0, \\ \Phi_{11} = A^T P_2 + P_2^T A + S + Q - R, \\ \Phi_{12} = P - P_2^T + A^T P_3, \\ \Phi_{22} = -P_3 - P_3^T + h^2 R. \end{cases} \quad (26)$$

Proof. Please see Appendix. \square

4.4. String Stability Analysis. The platoon system must ensure internal stability, meaning that each vehicle's error in terms of target longitudinal position, target velocity, and target acceleration should asymptotically converge to zero over time [49]. According to the paper [30], string stability can be demonstrated in various platoon communication topologies, such as the predecessor-leader-following topology, by utilizing the infinity norm. In addition, the s-domain-based analysis method is commonly used in the literature for linear platoons with typical communication topologies due to its theoretical convenience. Therefore, for the communication topology determined in this paper, the infinity norm as the foundation for proving string stability has been chosen. The condition for achieving string stability in the platoon is as follows:

$$\left\| \frac{E_i(j\omega)}{E_{i-1}(j\omega)} \right\|_{\infty} \leq 1, \forall \omega, \quad (27)$$

$$s^3 \tilde{P}_i(s) = -\alpha_1 s^2 \tilde{P}_i(s) + \alpha_2 e^{-\tau s} \tilde{P}_1(s) + \alpha_2 s e^{-\tau s} \tilde{P}_1(s) - \alpha_2 e^{-\tau s} \tilde{P}_i(s) - \alpha_2 s e^{-\tau s} \tilde{P}_i(s) + \alpha_3 e^{-\tau s} \tilde{P}_{i-1}(s) + \alpha_3 s e^{-\tau s} \tilde{P}_{i-1}(s). \quad (30)$$

We assume that the transfer function of the current vehicle and the leader vehicle is

$$G_i^1(s) \triangleq \frac{\alpha_2(1+s)e^{-\tau s}}{s^3 + \alpha_1 s^2 + \alpha_2(1+s)e^{-\tau s}}. \quad (31)$$

The transfer function of the current vehicle and the predecessor is represented as

$$\frac{E_{i+1}(s)}{E_i(s)} = \frac{\tilde{P}_{i+1}(s) - \tilde{P}_i(s)}{\tilde{P}_i(s) - \tilde{P}_{i-1}(s)} = \frac{G_i^1(s)\tilde{P}_1(s) + G_i^{i-1}(s)\tilde{P}_i(s) - G_i^1(s)\tilde{P}_1(s) - G_i^{i-1}(s)\tilde{P}_{i-1}(s)}{\tilde{P}_i(s) - \tilde{P}_{i-1}(s)} = \frac{G_i^{i-1}(s)(\tilde{P}_i(s) - \tilde{P}_{i-1}(s))}{\tilde{P}_i(s) - \tilde{P}_{i-1}(s)} = G_i^{i-1}(s). \quad (34)$$

Let $s = j\omega$, then the condition for string stability can be rewritten as the following equation. The platoon system satisfies string stability when the system satisfies the following equation:

$$\left\| G_i^{i-1}(j\omega) \right\|_{\infty} \leq 1, \forall \omega. \quad (35)$$

$$\omega^6 + \alpha_2^2 + \alpha_1^2 \omega^4 + \alpha_2^2 \omega^2 - 2\alpha_2 \omega^4 \cos(\tau\omega) + 2\alpha_2 \omega^3 \sin(\tau\omega) - 2\alpha_1 \alpha_2 \omega^3 \sin(\tau\omega) - 2\alpha_1 \alpha_2 \omega^2 \cos(\tau\omega) \geq \alpha_3^2 (1 + \omega^2), \quad (36)$$

where

where $E_i(j\omega)$ denotes the Laplace transform of the error of the spacing between the i th vehicle and the predecessor. Assuming that the communication time delay is a constant $\tau(t) = \tau$, then according to equation (15), the following equation exists:

$$\tilde{P}_{i,i-1}(t) = e_i(t) = \tilde{P}_i(t) - \tilde{P}_{i-1}(t). \quad (28)$$

The Laplace transform for the abovementioned equation is as follows:

$$E_i(s) = \tilde{P}_i(s) - \tilde{P}_{i-1}(s). \quad (29)$$

The Laplace transformation of equation (21) is represented as

$$G_i^{i-1}(s) \triangleq \frac{\alpha_3(1+s)e^{-\tau s}}{s^3 + \alpha_1 s^2 + \alpha_2(1+s)e^{-\tau s}}. \quad (32)$$

Then, we get

$$\tilde{P}_i(s) = G_i^1(s)\tilde{P}_1(s) + G_i^{i-1}(s)\tilde{P}_{i-1}(s). \quad (33)$$

By combining equations (27), (29), and (33), the following equation exists:

Considering the implications of Euler's formula and the infinite paradigm, the abovementioned formula can be rewritten as

$$\begin{aligned}\alpha_1 &= \frac{1}{\eta}, \\ \alpha_2 &= \frac{k_1 + k_2}{\eta}, \\ \alpha_3 &= \frac{k_2}{\eta}.\end{aligned}\quad (37)$$

$$\omega^6 + \omega^4(\alpha_1^2 - 2\alpha_2 - 2\alpha_1\alpha_2\tau - 2\alpha_2\tau) + \omega^2(\alpha_2^2 - 2\alpha_1\alpha_2 - \alpha_3^2) + (\alpha_2^2 - \alpha_3^2) \geq 0. \quad (38)$$

The conditions for the abovementioned equation to hold are as follows:

$$\begin{cases} \alpha_1^2 - 2\alpha_2 - 2\alpha_1\alpha_2\tau - 2\alpha_2\tau \geq 0, \\ \alpha_2^2 - 2\alpha_1\alpha_2 - \alpha_3^2 \geq 0, \\ \alpha_2^2 - \alpha_3^2 \geq 0. \end{cases} \quad (39)$$

By solving the abovementioned equation, the following parameter constraint bound can be derived:

$$\begin{cases} \eta \leq \frac{1}{2(k_1 + k_2)}, \\ \tau \leq \frac{1 - 2\eta(k_1 + k_2)}{(k_1 + k_2)(2 + \eta)}, \\ 0 \leq (k_1 - 2)k_1 + 2(k_1 - 1)k_2. \end{cases} \quad (40)$$

When the values k_1 , k_2 , η , and τ can satisfy the abovementioned conditions, then the platoon system could satisfy the string stability.

5. Simulations and Result Analysis

There are various simulation control platforms available for validating the CACC method [50]. In this paper, the proposed two-stage CACC method is verified and analyzed by using the MATLAB-TruckSim platform.

5.1. Simulation Scenario. In the simulation of this paper, the MATLAB-TruckSim simulation platform is used for joint simulation. The CAVP set up in this paper uses a heterogeneous platoon consisting of six trucks with different masses. Car1 means the leader, and car2 through car6 are the following vehicles. The parameters are set as shown in Table 2.

For the road section that features multiple slopes, this study selects a representative part from a real-life scenario to examine. The slope of this section is measured by using a total station. The road model is then integrated into TruckSim as part of the simulation scenario. Figure 4 depicts the overall characteristics of the road, with the altitude of its starting point being used as the reference

origin, where the horizontal coordinate is the position of the road point and the vertical coordinate is the elevation of the road.

Considering the trigonometric inequality $\cos(\tau\omega) \leq 1$, $\sin(\tau\omega) \leq \tau\omega$, $\sin(\tau\omega) \geq -\tau\omega$, equation (36) can be rewritten as

Since the DP algorithm discretizes the velocity, the boundaries of the velocity need to be set in this paper, and the lower limit of the velocity and the upper limit of the velocity are set to 30 km/h and 110 km/h, respectively. Also, considering that the acceleration of the vehicle in the process of driving should not be too large, the lower and upper limits of acceleration are set to -1.5 m/s^2 and 1.5. In the process of the DP algorithm optimization, if the average acceleration between the velocity of the current position and the velocity of the next position is greater than the set acceleration, the fuel consumption cost is set to INF, i.e., infinity.

In the design of the feedback controller, the control gain is chosen as $k_1 = 1.53$ and $k_2 = 0.68$. This selection ensures that the calculated upper limit of the delay, derived from internal stability, is $h = 141 \text{ ms}$, satisfying the requirements outlined in this paper. In addition, the initial positions of each vehicle within the platoon are defined as follows: 0 m for the leader, -10.5 m for the second vehicle, -36 m for the third vehicle, -57 m for the fourth vehicle, -75 m for the fifth vehicle, and -94 m for the sixth vehicle. The preset spacing in the platoon is $d_0 = 20 \text{ m}$.

5.2. Optimal Velocity Profiles and Fuel Consumption. In this paper, the velocity profiles with optimal energy consumption for the platoon in a multislope road are obtained by DP. To verify the effectiveness of the two-stage CACC method proposed in this paper, there are two benchmarks used as comparisons. One benchmark uses a constant speed cooperative adaptive cruise control (CS-CACC) method in which the platoon keeps a fixed speed. The other one uses model predictive control (MPC) as the controller of each vehicle in the platoon to follow the optimal velocity sequence. In the CS-CACC method, we perform a 1 km/h velocity discretization based on the upper and lower limits of the set velocity and simulate the overall fuel consumption of the platoon at different velocities. The results are shown in Figure 5(a). It can be seen that with the variation in vehicle velocity, the overall fuel consumption of the platoon shows a trend of first decreasing and then increasing. The constant velocity sequence with minimum energy consumption is

TABLE 2: Parameters for vehicles in the CAVP.

Car	Mass (kg)	ξ	C_d	$A_f (m)$	$r_i (m)$	$\eta (s)$	$\tau (ms)$
Car1	10000	0.95	0.69	6.8	0.51	0.1	120
Car2	8950	0.95	0.69	6.8	0.51	0.1	120
Car3	10340	0.95	0.69	6.8	0.52	0.1	120
Car4	9587	0.95	0.69	6.8	0.52	0.1	120
Car5	10240	0.95	0.69	6.8	0.53	0.1	120
Car6	9896	0.95	0.69	6.8	0.53	0.1	120

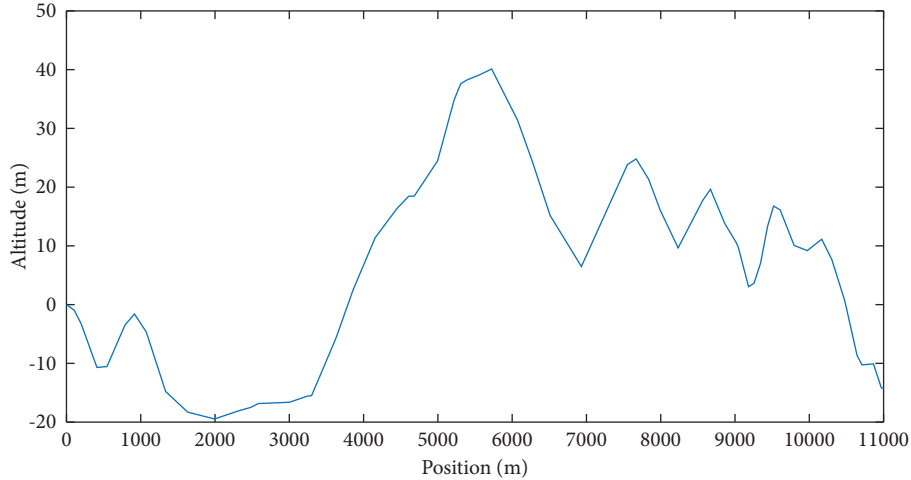


FIGURE 4: A road section for simulation.

50 km/h. The overall platoon fuel consumption is 13.2234 L. The velocity tracking error of the platoon during the simulation of constant velocity is shown in Figure 5(b). It can be seen that each vehicle in the platoon can effectively track the target velocity, and the absolute value of the error is kept within 0–0.45 m/s. Figure 5(c) represents the fuel consumption rate of the vehicles in the platoon driving using the CS-CACC strategy.

Figure 6 represents the simulation results of the platoon driving under the optimal velocity profiles optimized according to the DP algorithm. Figure 6(a) shows the optimal velocity profiles for the leader, and the maximum speed is 66.1 km/h. Figure 6(b) shows the velocity of the platoon during simulation, and it can be seen that each vehicle in the platoon can track the target velocity accurately. Also, due to the communication delay and actuator delay, the speed of the vehicles in the platoon fluctuates at the nodes where considerable acceleration changes in the optimal velocity profiles, but the controller designed in this paper can control the vehicles to return to the target velocity. Figure 6(c) represents the fuel consumption rate of the platoon during simulation.

Figure 7 represents the fuel consumption results of the platoon by using MPC. Figure 7(a) shows the velocity results of the platoon, and it can be seen that each vehicle in the platoon can track the target velocity accurately when using MPC. Each vehicle of the platoon except the leader will still have a lag when tracking the target velocity due to the

communication delay and actuator delay, but MPC controllers could bring each vehicle back to the target velocity. Figure 7(b) represents the fuel consumption rate of the platoon during the simulation.

To visualize the results of fuel consumption for the abovementioned three methods, the results are summarized in Table 3. According to Table 3, it can be seen that the results of the two-stage CACC have little difference when compared to the results of the MPC methods. Each vehicle of the platoon using two-stage CACC is reduced by 0.13%, 1.55%, -0.67%, -0.87%, -0.64%, and -0.77% when compared with the MPC methods, and the total fuel consumption is reduced by -0.21%. However, the fuel consumption results have a significant difference when comparing the two-stage CACC method with the CS-CACC method. Each vehicle in the platoon is reduced by 7.49%, 6.21%, 5.11%, 5.16%, 4.53%, and 3.59%, respectively. The overall fuel consumption is reduced by 5.33%. Therefore, the two-stage CACC strategy proposed in this paper can effectively reduce the fuel consumption of the platoon.

5.3. Tracking Controller Performance. To compare the differences in the results of the methods by using different controllers, the following parameters are used for comparison in this paper. They are the spacing error between each vehicle and the leader, the spacing error between each

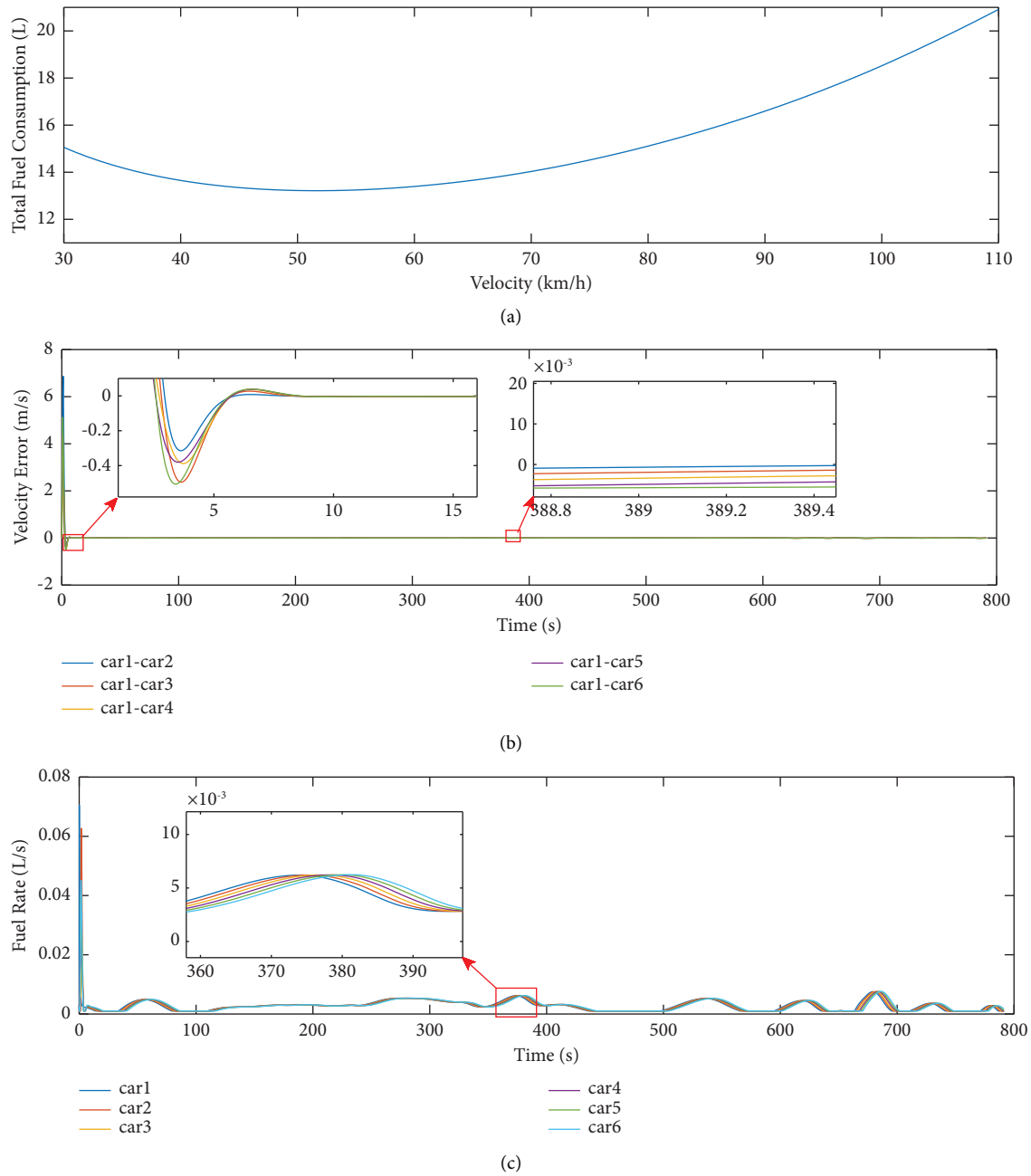
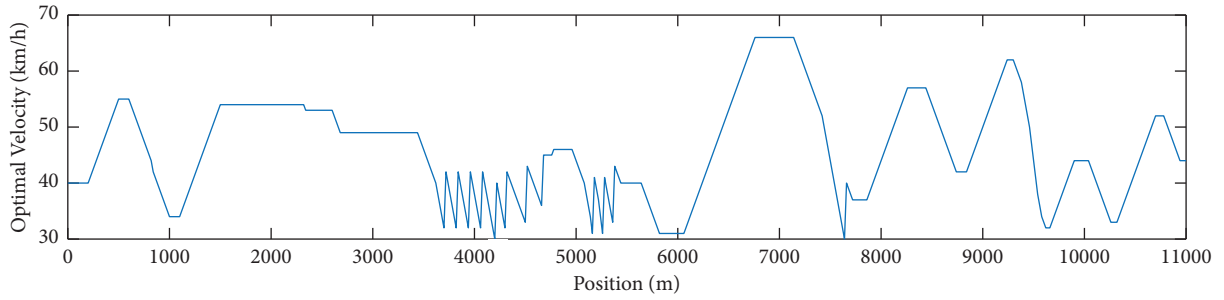


FIGURE 5: Simulation results of the platoon by using the CS-CACC strategy.

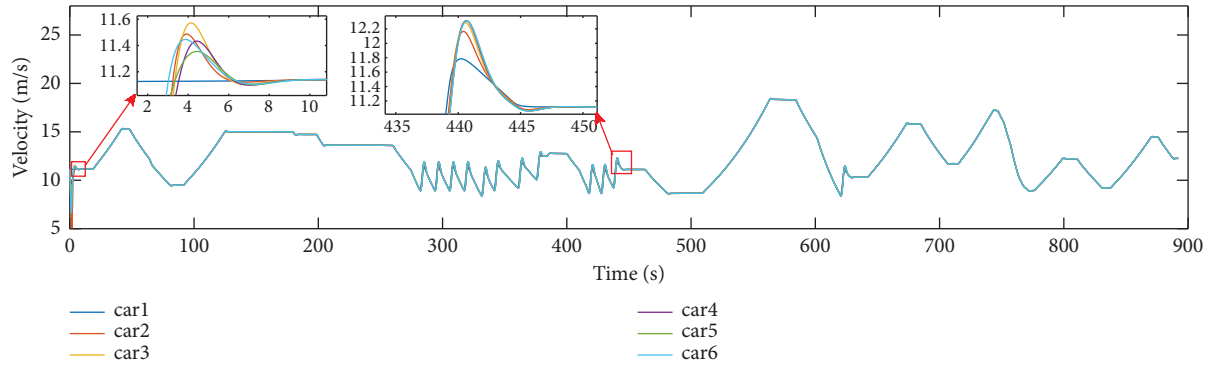
vehicle and the predecessor, the error between the actual velocity of the leader and the target velocity, the velocity error between each vehicle and the leader, and the velocity error between each vehicle and the predecessor, respectively. The results of the two-stage CACC method and MPC method are plotted in Figures 8–11. The results of CS-CACC, two-stage CACC, and MPC are statistically presented in Tables 4–7.

Figure 8 represents the results of the spacing error in the platoon by using the two-stage CACC method. Figure 8(a) represents the spacing error between each vehicle and the leader, and it can be seen that the results are significantly large in the simulation beginning because of the initial setup

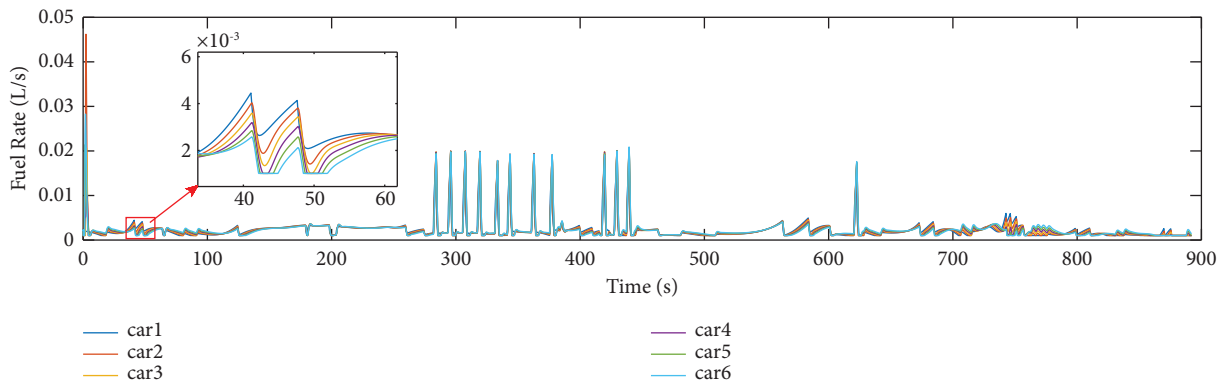
of the platoon, and then the spacing stays at the preset spacing at around 8 s. When the velocity of the leader changes, the spacing error between each vehicle and the leader will fluctuate, reaching about 0.84 m at the maximum, especially in the period from 300 s to 400 s. Figure 8(b) shows the results of the spacing error between each vehicle and the predecessor during the simulation. It has the same trend as Figure 8(a), but the maximum spacing error is smaller in the period from 300 s to 400 s. Figure 9 represents the results of the spacing error in the platoon by using the MPC method. It can be seen that the results of the spacing error by using the MPC method are larger than those using the two-stage CACC method. Figure 9(a) represents the spacing errors



(a)

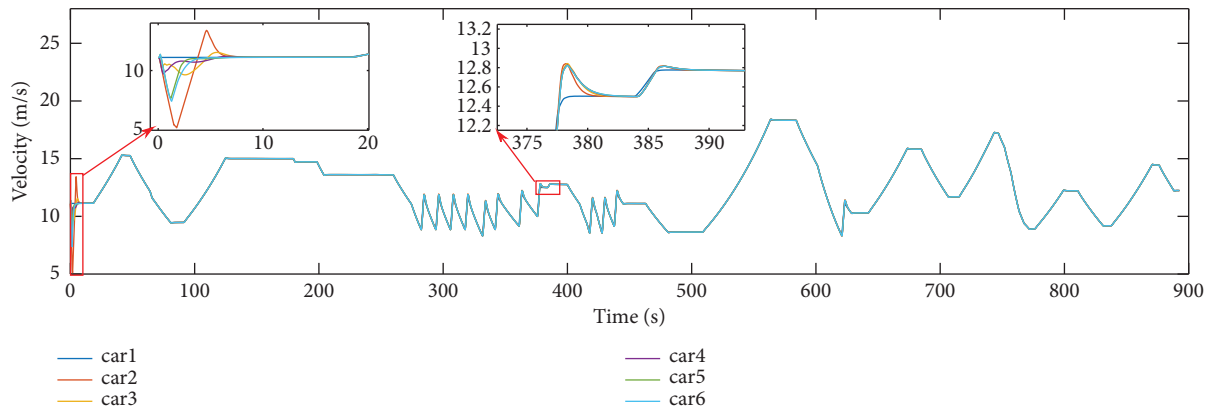


(b)



(c)

FIGURE 6: Simulation results of the platoon by using the two-stage CACC strategy.



(a)

FIGURE 7: Continued.

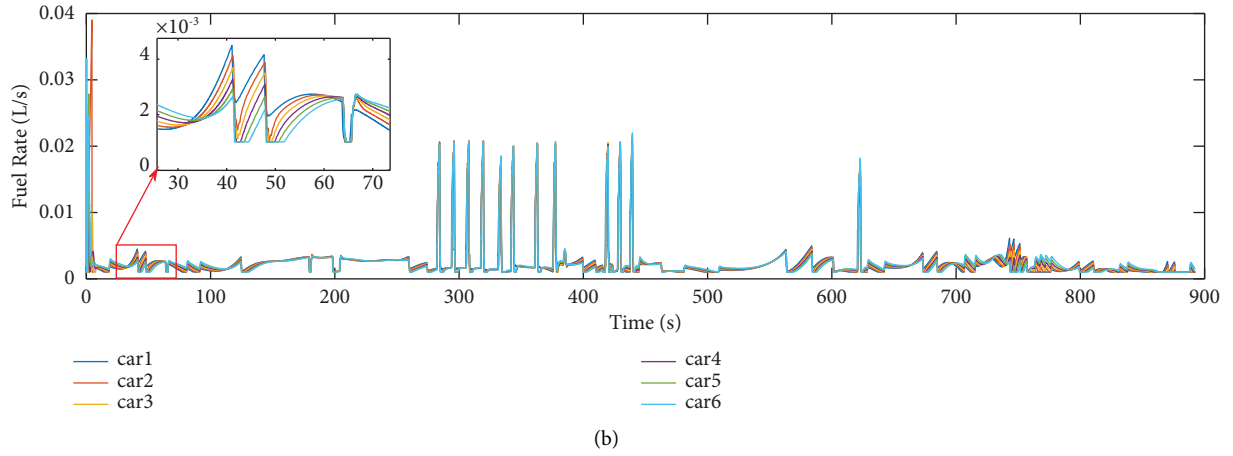


FIGURE 7: Simulation results of the platoon by using MPC.

TABLE 3: Comparison results of fuel consumption (L).

Car	Car1	Car2	Car3	Car4	Car5	Car6	Total
CS-CACC	2.1821	2.2221	2.1908	2.1947	2.2127	2.2209	13.2234
Two-stage CACC	2.0299	2.0921	2.0841	2.0869	2.1167	2.1438	12.5536
MPC	2.0326	2.1252	2.0702	2.0689	2.1031	2.1273	12.5273

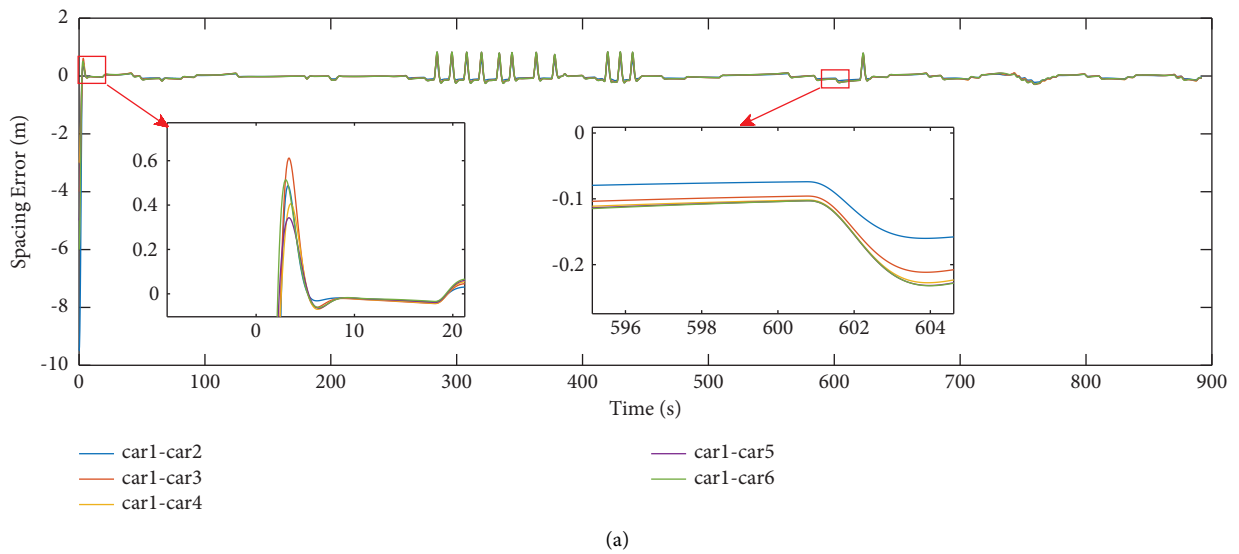


FIGURE 8: Continued.

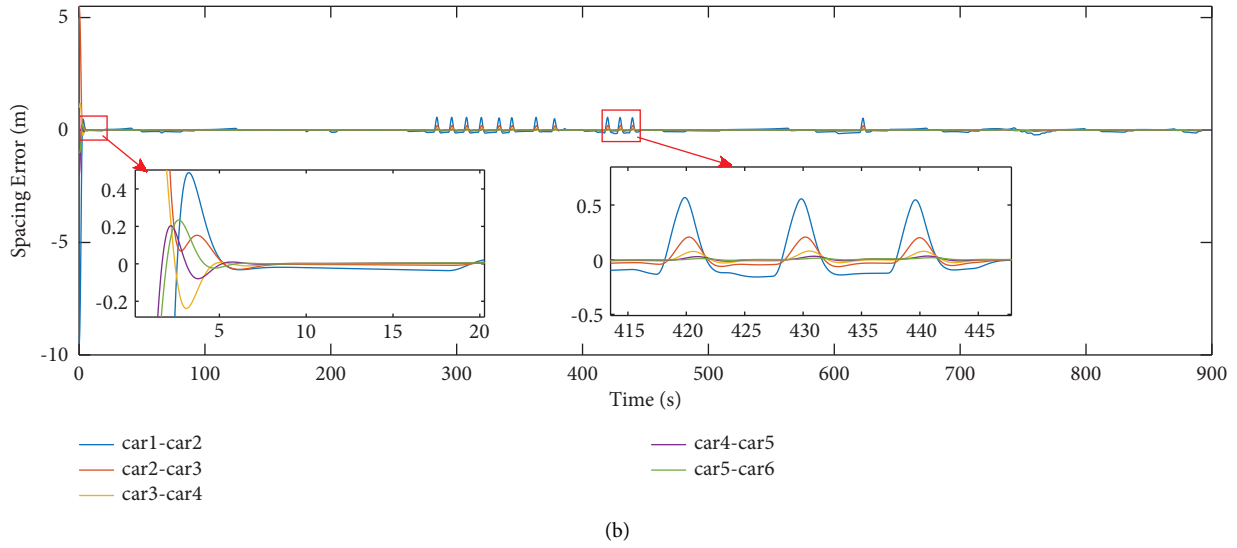


FIGURE 8: Results of spacing error in the simulation by using the two-stage CACC strategy.

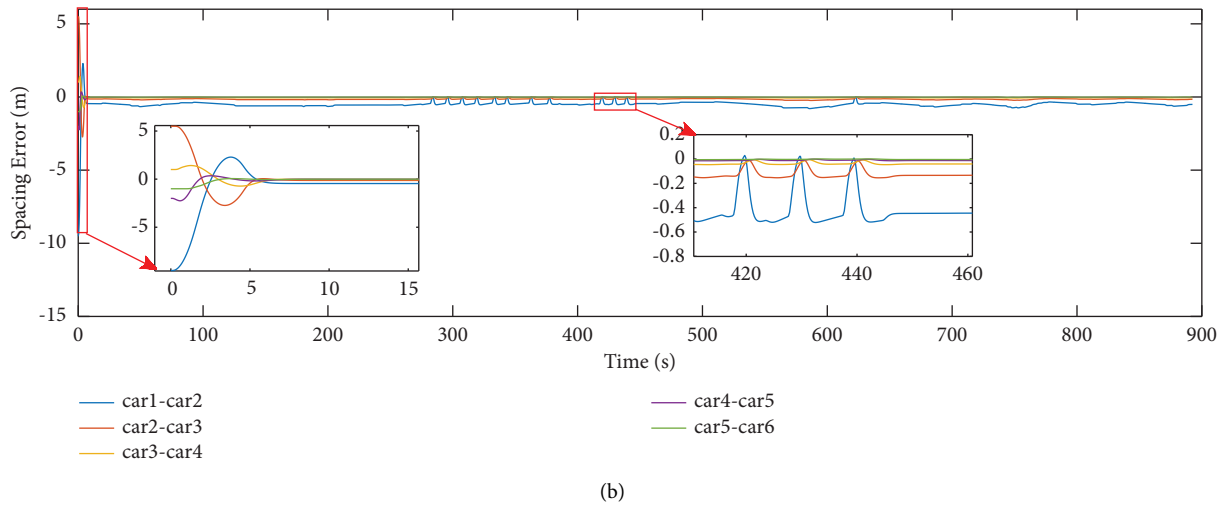
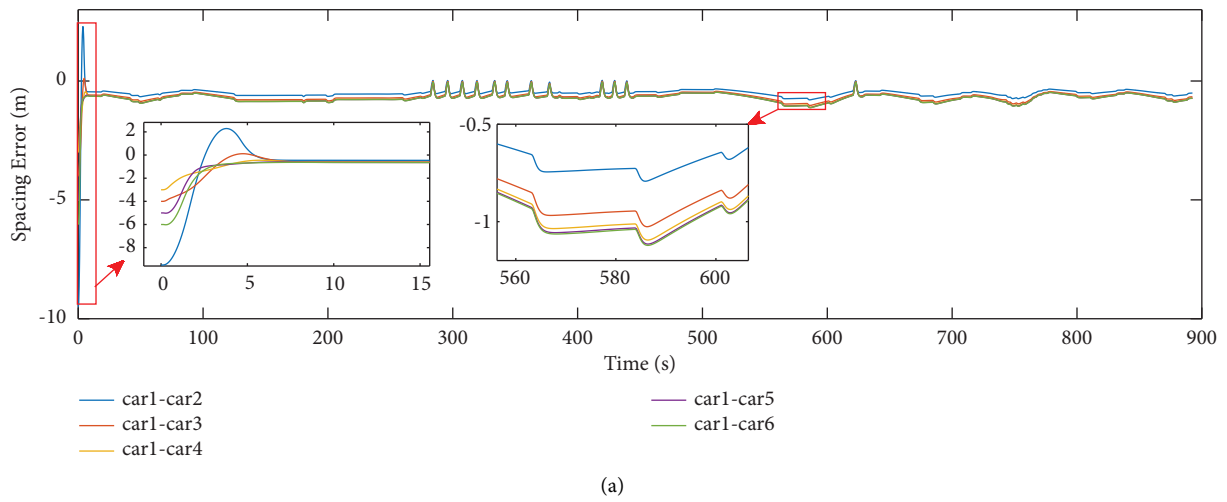


FIGURE 9: Results of spacing error in the simulation by using MPC.

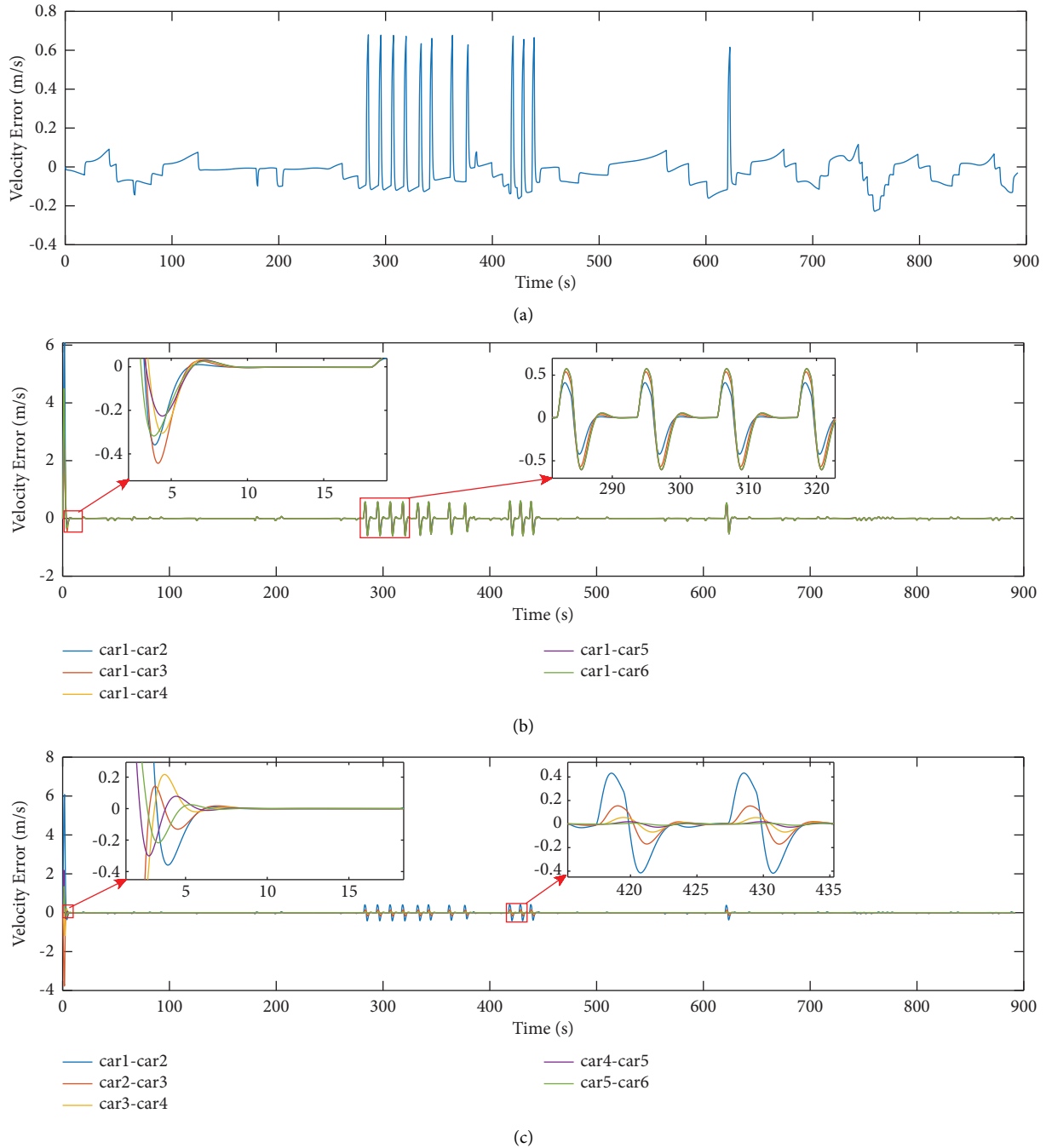


FIGURE 10: Results of velocity tracking error in the simulation by using the two-stage CACC strategy.

between vehicles and the leader vehicle. Figure 9(b) shows the results of the spacing error between each vehicle and the predecessor and there is a phenomenon in both Figures 8 and 9. As the vehicle sequence number increases, the spacing error between each vehicle and the leader would increase, but the spacing error between each vehicle and the predecessor would decrease.

To visualize the difference in the spacing error of the CS-CACC method, two-stage method, and MPC method, the results of the root mean square, maximum and minimum values, are shown in Tables 4 and 5. Table 4 represents

the results of the spacing error between each vehicle and the leader. Table 5 represents the results of spacing error between each vehicle and the predecessor.

As can be seen from Tables 4 and 5, whether it is in the results of spacing error between each vehicle and the leader or in the results of spacing error between each vehicle and the predecessor, the order of effectiveness is the CS-CACC method, the two-stage CACC method, and the MPC method, respectively. The MPC method has a lower accuracy in spacing tracking when compared to the other two methods. This might be caused by the reason that the MPC

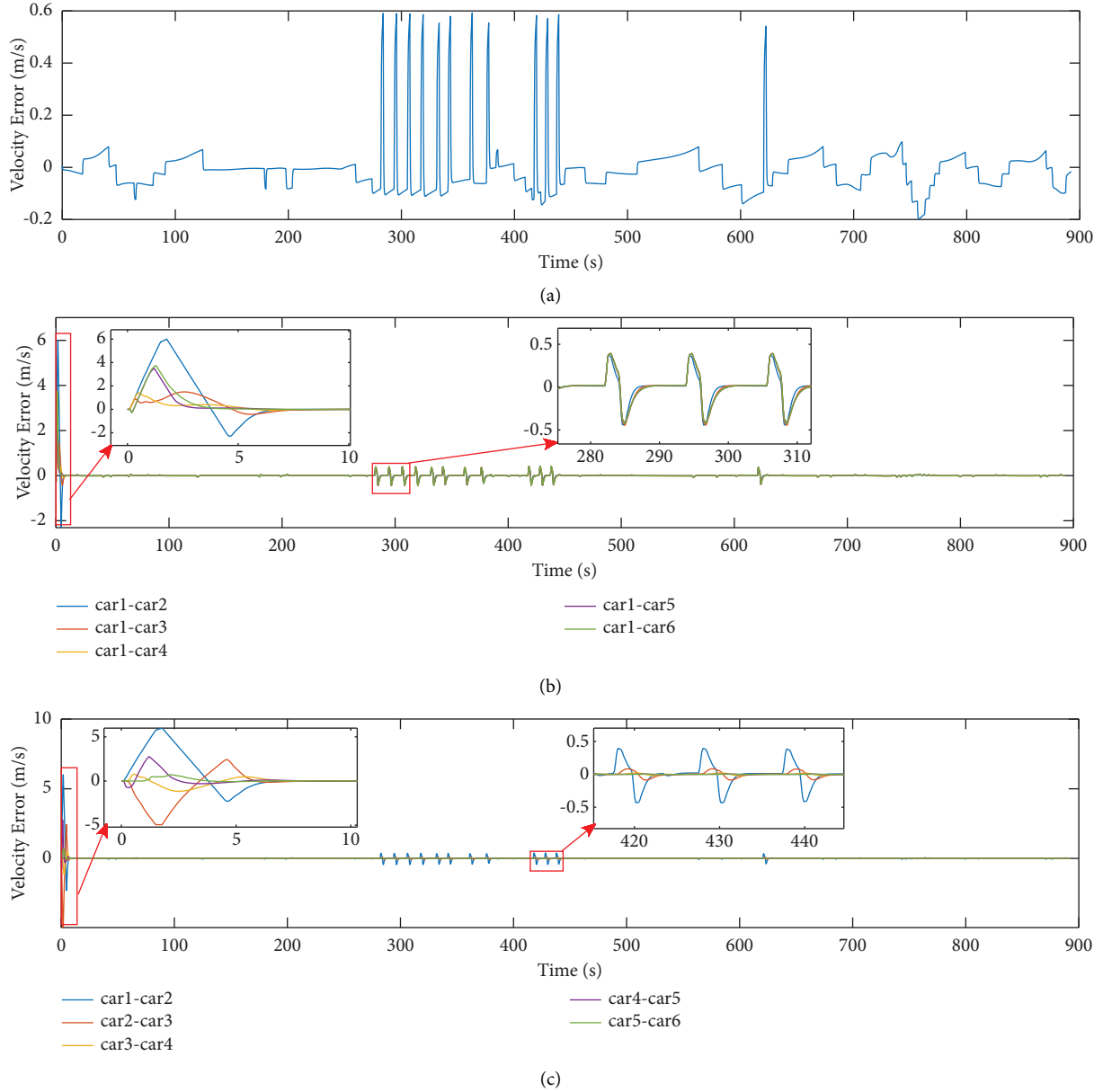


FIGURE 11: Results of velocity tracking error in the simulation by using MPC.

TABLE 4: Results of spacing error between each vehicle and the leader.

		car1-car2	car1-car3	car1-car4	car1-car5	car1-car6
CS-CACC	Root mean square	0.1014	0.0177	0.0089	0.0228	0.0346
	Maximum	0.4245	0.7194	0.5871	0.6107	0.7623
	Minimum	-9.5	-4	-3	-5	-6
Two-stage CACC	Root mean square	0.1273	0.0394	0.0303	0.0465	0.0602
	Maximum	0.5683	0.7626	0.8228	0.8386	0.8414
	Minimum	-9.5	-4	-3	-5	-6
MPC	Root mean square	0.3943	0.4704	0.5165	0.5562	0.5803
	Maximum	2.2899	0.1153	-0.0347	-0.0441	-0.0469
	Minimum	-9.5	-4	-3	-5.0236	-6.0236

TABLE 5: Results of spacing error between each vehicle and the predecessor.

		car1-car2	car2-car3	car3-car4	car4-car5	car5-car6
CS-CACC	Root mean square	0.1014	0.0373	0.0022	0.0037	0.0013
	Maximum	0.4245	5.5	1.1446	0.0632	0.1517
	Minimum	-9.5	-0.03272	-0.13928	-2	-1
Two-stage CACC	Root mean square	0.1273	0.0396	0.0026	0.0038	0.0015
	Maximum	0.5683	5.5	1.1877	0.2038	0.2342
	Minimum	-9.5	-0.062	-0.2387	-2	-1
MPC	Root mean square	0.3943	0.0751	0.0068	0.0062	0.0020
	Maximum	2.2899	5.5	1.4145	0.3506	0.0572
	Minimum	-9.5	-2.7331	-0.7223	-2.2518	-1

TABLE 6: Velocity errors between each vehicle and the leader.

		car1	car2	car3	car4	car5	car6
CS-CACC	Root mean square	0.0030	0.0615	0.0128	0.0085	0.0226	0.0317
	Maximum	2.7779	6.8635	2.5513	2.5296	4.4174	5.1236
	Minimum	-0.0680	-0.3146	-0.4954	-0.3884	-0.3804	-0.5062
Two-stage CACC	Root mean square	0.0120	0.0557	0.0198	0.0167	0.0273	0.0354
	Maximum	0.6795	6.079	2.388	1.5474	3.7232	4.493
	Minimum	-0.2279	-0.4231	-0.5679	-0.6042	-0.6071	-0.6042
MPC	Root mean square	0.0094	0.0644	0.0102	0.0069	0.0157	0.0189
	Maximum	0.5925	6.0091	1.4888	1.4108	3.5035	3.7460
	Minimum	-0.1991	-2.3096	-0.4464	-0.4284	-0.4242	-0.4238

TABLE 7: Velocity errors between each vehicle and the predecessor.

		car1	car2	car3	car4	car5	car6
CS-CACC	Root mean square	0.0030	0.0615	0.0193	0.0013	0.0036	0.0010
	Maximum	2.7779	6.8635	0.0192	0.3105	1.9083	0.9557
	Minimum	-0.0680	-0.3146	-4.3157	-1.1101	-0.1330	-0.1336
Two-stage CACC	Root mean square	0.0120	0.0557	0.0181	0.0016	0.0037	0.0013
	Maximum	0.6795	6.079	0.1552	0.3354	2.1864	1.3469
	Minimum	-0.2279	-0.4231	-3.7721	-1.1799	-0.3007	-0.2173
MPC	Root mean square	0.0094	0.0644	0.0382	0.0026	0.0058	0.0005
	Maximum	0.5925	6.0091	2.4304	0.7670	2.7704	0.7141
	Minimum	-0.1991	-2.3096	-4.9656	-1.1620	-0.7538	-0.0675

method does not consider time delays. In the results of spacing error between each vehicle and the leader, the minimum values of the root mean square are 0.0089 for car1 and car4 using CS-CACC, 0.0303 for car1 and car4 using two-stage CACC, and 0.3943 for car1 and car2 using MPC. In the results of spacing error between each vehicle and the predecessor, the minimum values of the root mean square are 0.0013 for car5 and car6 using CS-CACC, 0.0015 for car5 and car6 using two-stage CACC, and 0.0020 for car5 and car6 using MPC. This shows that the spacing tracking accuracy of the abovementioned methods is higher when using the target spacing from the leader than using the target spacing from the predecessor.

Figure 10 represents the results of velocity error by using the two-stage CACC method. Figure 10(a) represents the velocity error between the leader and the optimal velocity sequence. The maximum velocity error occurs in the period from 300 s to 400 s, and the value is 0.6795. The results show that the leader could track the optimal velocity sequence well. Figure 10(b) represents the velocity

error between each vehicle and the leader. Figure 10(c) represents the velocity error between each vehicle and the predecessor. Similar to the trend in the spacing error, the velocity error of the following vehicle rises significantly during periods when the velocity of the leader changes more frequently. And as the vehicle number rises, the velocity error increases with the leader as the reference and decreases with the predecessor as the reference. And it can be seen that compared to the velocity error with the leader, the velocity error between each vehicle and the predecessor is smaller. Figure 11 represents the results of velocity error by using the MPC method. Figure 11(a) represents the velocity error between the leader and the optimal velocity sequence. The maximum velocity error occurs in the period from 300 s to 400 s, and the value is 0.5925. Figure 11(b) represents the velocity error between each vehicle and the leader. Figure 11(c) represents the velocity error between each vehicle and the predecessor. The results have the same trend when compared to the two-stage CACC method.

Tables 6 and 7 show the results of velocity error by using the CS-CACC method, two-stage method, and MPC method. Table 6 represents the results of velocity error between each vehicle and the leader. Table 7 represents the results of velocity error between each vehicle and the predecessor.

As can be seen from Tables 6 and 7, unlike the trend in the results of spacing error, three methods have their advantages and disadvantages over vehicle speed tracking. The CS-CACC method has the best performance of tracking the target velocity for the leader with the root mean square value of 0.0030, and the two-stage method has the best performance of tracking the target velocity for car2 with the root mean square value of 0.0557. When using the velocity of the leader as the reference, the MPC method has the best performance of tracking the target velocity for car3 through car6 with the root mean square values of 0.0102, 0.0069, 0.0157, and 0.0189. However, when using velocity of the predecessor as the reference, the CS-CACC method has the best performance of tracking the target velocity for car4 and car5 with the root mean square values of 0.0013 and 0.0036, and the two-stage CACC method has the best performance of tracking the target velocity for car3 with the root mean square value of 0.0181, and the MPC method has the best performance of tracking the target velocity for car6 with the root mean square value of 0.0005. In the results of velocity error, using the velocity of the predecessor as the reference has smaller values than using the velocity of the leader as the reference. Although the performance of the two-stage CACC method is not the best in velocity tracking, it is still able to track the optimal velocity sequence effectively.

The abovementioned results show that the two-stage CACC method proposed in this paper can lead to a significant reduction in fuel consumption when the platoon is driving on a multislope road section. Also, considering the communication delay and actuator delay of the platoon, the feedback controller designed in this paper can make the platoon track the target spacing and the optimal velocity sequence effectively, which is consistent with the global internal stability and string stability of the platoon.

6. Conclusions

This paper proposes a two-stage CACC method for CAVPs in a platoon cruising scenario on multislope road sections. In the first stage, a DP algorithm is utilized to plan global optimal velocity profiles for the platoon. In the second stage, a feedback controller is developed for each vehicle, considering the communication delay and actuator delay. The gain parameters are bounded and fulfill the conditions for global internal stability and string stability. The proposed two-stage CACC method is simulated by using road section data, thereby validating the global internal stability and string stability of the platoon. Under a fixed delay condition, the platoon effectively maintains the predefined spacing and tracks the optimal velocity profiles. Comparisons with the CS-CACC method and the MPC method demonstrate a significant reduction in fuel consumption of 5.33% compared to the CS-CACC method, with a marginal increase of -0.21% in fuel consumption when compared to the MPC method.

However, because of the limitations of experimental conditions and scenarios, real-vehicle experiments were not performed. Therefore, validation is limited to simulations in this paper. Future research will consider traffic factors and complex scenarios to facilitate validation under real-vehicle conditions. It is noteworthy that although a fixed and known time delay is used in this paper, uncertainties exist in platoon delays in complex conditions and extreme environments. In addition, there is a risk of packet loss during communication. Therefore, future research will focus on addressing these uncertainties and improving the platoon's adaptability in various environments.

Appendix

The proof of Section 5.3 is as follows. If there exist matrices $(P, Q, S, R, P_2, P_3) \in \mathbb{R}^{3n \times 3n}$ satisfied (26), P, Q, S, R are positive definite matrices, and P_2 and P_3 are matrices of proper dimension, then the e system is asymptotically stable. Consider the Lyapunov-Krasovskii function candidate as

$$V(t, x(t), \dot{x}(t)) = x^T(t)Px(t) + \int_{t-h}^t x^T(s)Sx(s)ds + h \int_{-h}^0 \int_{t-h}^t \dot{x}^T(s)R\dot{x}(s)ds d\theta + \int_{t-\tau(t)}^t x^T(s)Qx(s)ds. \quad (\text{A.1})$$

The time derivative of (A.1) is as follows:

$$\begin{aligned} \frac{d}{dt}V &= 2x^T(t)P\dot{x}(t) + h^2\dot{x}^T(t)R\dot{x}(t) - h \int_{t-h}^t \dot{x}^T(s)R\dot{x}(s)ds + x^T(t)[S+Q]x(t) - x^T(t-h)Sx(t-h) \\ &\quad - (1 - \dot{\tau}(t))x^T(t-\tau(t))Qx(t-\tau(t)). \end{aligned} \quad (\text{A.2})$$

Consider the following equation:

$$-h \int_{t-h}^t \dot{x}^T(s) R \dot{x}(s) ds = -h \int_{t-h}^{t-\tau(t)} \dot{x}^T(s) R \dot{x}(s) ds - h \int_{t-\tau(t)}^t \dot{x}^T(s) R \dot{x}(s) ds. \quad (\text{A.3})$$

Based on Jensen's inequality, (A.3) could be rewritten as follows:

$$-h \int_{t-h}^t \dot{x}^T(s) R \dot{x}(s) ds \leq - \int_{t-h}^{t-\tau(t)} \dot{x}^T(s) ds R \int_{t-h}^{t-\tau(t)} \dot{x}(s) ds - \int_{t-\tau(t)}^t \dot{x}^T(s) ds R \int_{t-\tau(t)}^t \dot{x}(s) ds. \quad (\text{A.4})$$

By applying the Newton–Leibniz formula, the following equation exists:

$$0 = 2 \left[x^T(t) P_2^T + \dot{x}^T(t) P_3^T \right] [Ax(t) + Bx(t - \tau(t)) - \dot{x}(t)]. \quad (\text{A.5})$$

By combining with (A.2), (A.4), and (A.5), the following equation exists:

$$\begin{aligned} \frac{d}{dt} V \leq & 2x^T(t) P \dot{x}(t) + h^2 \dot{x}^T(t) R \dot{x}(t) - [x(t) - x(t - \tau(t))]^T R [x(t) - x(t - \tau(t))] \\ & - [x(t - \tau(t)) - x(t - h)]^T R [x(t - \tau(t)) - x(t - h)] + x^T(t) [S + Q] x(t) - x^T(t - h) S x(t - h) \\ & - (1 - \varphi) x^T(t - \tau(t)) Q x(t - \tau(t)) + 2 \left[x^T(t) P_2^T + \dot{x}^T(t) P_3^T \right] [Ax(t) + Bx(t - \tau(t)) - \dot{x}(t)]. \end{aligned} \quad (\text{A.6})$$

Let $\xi_d(t) = [x(t), \dot{x}(t), x(t - h), x(t - \tau(t))]^T$, (A.6) could be rewritten as follows:

$$\frac{d}{dt} V \leq \xi_d^T(t) \Phi_d \xi_d(t), \quad (\text{A.7})$$

where Φ_d is described in (26). When $\Phi_d < 0$, there exists an infinitesimal number $\alpha > 0$ holding the equation $\dot{V} < -\alpha \|x(t)\|^2$, and system (24) is asymptotically stable. Then, the proof of Section 5.3 has been completed.

Data Availability

The data that support the findings of this study are available from the corresponding author upon reasonable request.

Conflicts of Interest

The authors declare that they have no conflicts of interest regarding the publication of this paper.

Acknowledgments

This work was supported by the 111 Project, China (grant no. B17034), the Innovative Research Team Development Program of the Ministry of Education of China (grant no.

IRT_17R83), the Great Project of Hubei Province Technological Innovation (grant no. 2020DEB014), the Hubei Key Laboratory of Advanced Technology for Automotive Components and Hubei Collaborative Innovation Center for Automotive Components Technology, and the Wuhan University of Technology, Wuhan 430070, China.

References

- [1] C. Zou, *Modeling and Control of Vehicle Cooperative Adaptive Cruise System*, Dalian University of Technology, Liaoning, China, 2020, in Chinese.
- [2] S. Yang, S. E. Shladover, X.-Y. Lu, H. Ramezani, A. Kailas, and O. D. Altan, "A bayesian regression analysis of truck drivers' use of cooperative adaptive cruise control (CACC) for platooning on California highways," *Journal of Intelligent Transportation Systems*, vol. 27, no. 1, pp. 80–91, 2021.
- [3] Y. Weng, R. Salehi, X. Ge et al., "Model-free speed management for a heterogeneous platoon of connected ground vehicles," *Journal of Intelligent Transportation Systems*, vol. 26, no. 2, pp. 183–197, 2020.
- [4] L. Zhang, F. Chen, X. Ma, and X. Pan, "Fuel economy in truck platooning: a literature overview and directions for future research," *Journal of Advanced Transportation*, vol. 2020, Article ID 2604012, pp. 1–10, 2020.
- [5] S. Lu, Y. Cai, L. Chen, H. Wang, X. Sun, and H. Gao, "Altruistic cooperative adaptive cruise control of mixed traffic

- platoon based on deep reinforcement learning,” *IET Intelligent Transport Systems*, vol. 17, no. 10, pp. 1951–1963, 2023.
- [6] H. Liu, X.-Y. Lu, and S. E. Shladover, “Mobility and energy consumption impacts of cooperative adaptive cruise control vehicle strings on freeway corridors,” *Transportation Research Record: Journal of the Transportation Research Board*, vol. 2674, no. 9, pp. 111–123, 2020.
 - [7] L. Zhu, Y. Tang, and D. Yang, “Cellular automata-based modeling and simulation of the mixed traffic flow of vehicle platoon and normal vehicles,” *Physica A: Statistical Mechanics and Its Applications*, vol. 584, Article ID 126368, 2021.
 - [8] Z. Yao, Y. Wu, Y. Wang, B. Zhao, and Y. Jiang, “Analysis of the impact of maximum platoon size of cavs on mixed traffic flow: an analytical and simulation method,” *Transportation Research Part C: Emerging Technologies*, vol. 147, 2023.
 - [9] C. Sun, J. Guanetti, F. Borrelli, and S. J. Moura, “Optimal eco-driving control of connected and autonomous vehicles through signalized intersections,” *IEEE Internet of Things Journal*, vol. 7, no. 5, pp. 3759–3773, 2020.
 - [10] C. Zhai, C. Chen, X. Yang et al., “Ecological driving for connected and automated vehicles at unsaturated intersections considering queue effects,” *IEEE Transactions on Vehicular Technology*, vol. 71, no. 12, Article ID 12552, 2022.
 - [11] X. Song, Y. Sun, H. Li, B. Liu, and Y. Cao, “Ecological cooperative adaptive control of connected automate vehicles in mixed and power-heterogeneous traffic flow,” *Electronics*, vol. 12, pp. 2158–2210, 2023.
 - [12] H. Liu, X.-Y. Lu, and S. E. Shladover, “Traffic signal control by leveraging cooperative adaptive cruise control (CACC) vehicle platooning capabilities,” *Transportation Research Part C: Emerging Technologies*, vol. 104, pp. 390–407, 2019.
 - [13] O. Pauca, A. Maxim, and C. F. Caruntu, “Communication topologies evaluation for a vehicle merging into a platoon on highway,” in *Proceedings of the 2022 30th Mediterranean Conference on Control and Automation (MED)*, Vouliagmeni, Greece, June 2022.
 - [14] S. Woo and A. Skabardonis, “Flow-aware platoon formation of connected automated vehicles in a mixed traffic with human-driven vehicles,” *Transportation Research Part C: Emerging Technologies*, vol. 133, Article ID 103442, 2021.
 - [15] G. Lee and J.-I. Jung, “Decentralized platoon join-in-middle protocol considering communication delay for connected and automated vehicle,” *Sensors*, vol. 21, pp. 7126–7221, 2021.
 - [16] Z. Gao, Z. Wu, W. Hao, K. Long, Y.-J. Byon, and K. Long, “Optimal trajectory planning of connected and automated vehicles at on-ramp merging area,” *IEEE Transactions on Intelligent Transportation Systems*, vol. 23, no. 8, Article ID 12675, 2022.
 - [17] F. Ma, Y. Yang, J. Wang et al., “Eco-driving-based cooperative adaptive cruise control of connected vehicles platoon at signalized intersections,” *Transportation Research Part D: Transport and Environment*, vol. 92, Article ID 102746, 2021.
 - [18] J. Bas, J. L. Zofío, C. Cirillo, H. Chen, and H. A. Rakha, “Policy and industry implications of the potential market penetration of electric vehicles with eco-cooperative adaptive cruise control,” *Transportation Research Part A: Policy and Practice*, vol. 164, pp. 242–256, 2022.
 - [19] C. Guo, C. Fu, R. Luo, and G. Yang, “Energy-oriented car-following control for a front- and rear-independent-drive electric vehicle platoon,” *Energy*, vol. 257, Article ID 124732, 2022.
 - [20] C. Zhai, X. Chen, C. Yan, Y. Liu, and H. Li, “Ecological cooperative adaptive cruise control for a heterogeneous platoon of heavy-duty vehicles with time delays,” *IEEE Access*, vol. 8, Article ID 146208, 2020.
 - [21] C. Zhai, C. Chen, X. Zheng et al., “Ecological cooperative adaptive cruise control for heterogeneous vehicle platoons subject to time delays and input saturations,” *IEEE Transactions on Intelligent Transportation Systems*, vol. 24, no. 3, pp. 2862–2873, 2023.
 - [22] X. Song, F. Ding, F. Xiao, and D. He, “Data-driven optimal cooperative adaptive cruise control of heterogeneous vehicle platoons with unknown dynamics,” *Science China Information Sciences*, vol. 63, no. 9, Article ID 190204, 2020.
 - [23] C. Flores, J. Spring, D. Nelson, S. Iliev, and X.-Y. Lu, “Enabling cooperative adaptive cruise control on strings of vehicles with heterogeneous dynamics and powertrains,” *Vehicle System Dynamics*, vol. 61, no. 1, pp. 128–149, 2022.
 - [24] Z. Yang, J. Huang, D. Yang, and Z. Zhong, “Collision-free ecological cooperative robust control for uncertain vehicular platoons with communication delay,” *IEEE Transactions on Vehicular Technology*, vol. 70, no. 3, pp. 2153–2166, 2021.
 - [25] V. Turri, B. Besselink, and K. H. Johansson, “Cooperative look-ahead control for fuel-efficient and safe heavy-duty vehicle platooning,” *IEEE Transactions on Control Systems Technology*, vol. 25, no. 1, pp. 12–28, 2017.
 - [26] Q. Wang, *Speed Optimization and Cooperative Control of Transport Platoon*, Dalian University of Technology, Liaoning, China, 2019, in Chinese.
 - [27] D. Xia, B. Li, J. Zhang, B. Zhang, and N. Zhang, “Ecological cooperative adaptive cruise control of over-actuated electric vehicles with in-wheel motor in traffic flow,” *IET Intelligent Transport Systems*, vol. 15, no. 6, pp. 765–780, 2021.
 - [28] S. Badnava, N. Meskin, A. Gastli et al., “Platoon transitional maneuver control system: a review,” *IEEE Access*, vol. 9, Article ID 88327, 2021.
 - [29] J. Chen, J. H. Park, S. Xu, and B. Zhang, “A survey of inequality techniques for stability analysis of time-delay systems,” *International Journal of Robust and Nonlinear Control*, vol. 32, no. 11, pp. 6412–6440, 2022.
 - [30] S. Feng, Y. Zhang, S. E. Li, Z. Cao, H. X. Liu, and L. Li, “String stability for vehicular platoon control: definitions and analysis methods,” *Annual Reviews in Control*, vol. 47, pp. 81–97, 2019.
 - [31] Y. Yang, F. Ma, J. Wang et al., “Cooperative ecological cruising using hierarchical control strategy with optimal sustainable performance for connected automated vehicles on varying road conditions,” *Journal of Cleaner Production*, vol. 275, Article ID 123056, 2020.
 - [32] J. Fan, Y. Li, H. Zhu, and S. Yu, “Longitudinal control of connected truck platoon based on prescan,” in *2021 33rd Chinese Control and Decision Conference (CCDC)*, pp. 1110–1115, Kunming, China, May 2021.
 - [33] Y. Zhang, Y. Bai, M. Wang, and J. Hu, “Cooperative adaptive cruise control with robustness against communication delay: an approach in the space domain,” *IEEE Transactions on Intelligent Transportation Systems*, vol. 22, no. 9, pp. 5496–5507, 2021.
 - [34] H. Liu, *Based on Transient Polynomial Fuel Consumption Model and Model Predictive Control*, Jilin University, Changchun, China, 2018, in Chinese.
 - [35] J. Wang and H. A. Rakha, “Fuel consumption model for heavy duty diesel trucks: model development and testing,” *Transportation Research Part D: Transport and Environment*, vol. 55, pp. 127–141, 2017.
 - [36] Y. Zhisheng, *Automobile Theory*, China Machine Press, Danyang, China, 2019, in Chinese.

- [37] Q. Qin, X. Liu, H. Wang, and X. Wang, "Research progress of aerodynamics performance in vehicle platoon," *Automobile Applied Technology*, vol. 47, no. 8, pp. 188–204, 2022, in Chinese.
- [38] Y. Zheng, *Dynamic Modeling and Distributed Control of Vehicular Platoon under the Four-Component Framework*, Tsinghua University, Beijing, China, 2015, in Chinese.
- [39] Y. Dai, Y. Yang, H. Zhong, H. Zuo, Q. Zhang, and L. Zhu, "Stability and safety of cooperative adaptive cruise control vehicular platoon under diverse information flow topologies," *Wireless Communications and Mobile Computing*, vol. 2022, pp. 1–28, 2022.
- [40] H. Long, A. Khalatbarisoltani, and X. Hu, "MPC-based eco-platooning for homogeneous connected trucks under different communication topologies," *2022 IEEE Intelligent Vehicles Symposium (IV)*, pp. 241–246, 2022.
- [41] E. Fridman, "Introduction to time-delay systems analysis and control," *Systems and Control: Foundations Systems and Control: Foundations and Applications*, 2014.
- [42] Y. Zhang, Y. Bai, J. Hu, and M. Wang, "Control design, stability analysis, and traffic flow implications for cooperative adaptive cruise control systems with compensation of communication delay," *Transportation Research Record: Journal of the Transportation Research Board*, vol. 2674, no. 8, pp. 638–652, 2020.
- [43] Y. Liu, C. Pan, H. Gao, and G. Guo, "Cooperative spacing control for interconnected vehicle systems with input delays," *IEEE Transactions on Vehicular Technology*, vol. 66, no. 12, Article ID 10692, 2017.
- [44] H. Xing, J. Ploeg, and H. Nijmeijer, "Compensation of communication delays in a cooperative acc system," *IEEE Transactions on Vehicular Technology*, vol. 69, no. 2, pp. 1177–1189, 2020.
- [45] G. Guo, P. Li, and L. Y. Hao, "A new quadratic spacing policy and adaptive fault-tolerant platooning with actuator saturation," *IEEE Transactions on Intelligent Transportation Systems*, vol. 23, no. 2, pp. 1200–1212, 2022.
- [46] Y. Liu and W. Wang, "A safety reinforced cooperative adaptive cruise control strategy accounting for dynamic vehicle-to-vehicle communication failure," *Sensors*, vol. 21, pp. 6158–6218, 2021.
- [47] Y.-C. Lin and H. L. T. Nguyen, "Adaptive neuro-fuzzy predictor-based control for cooperative adaptive cruise control system," *IEEE Transactions on Intelligent Transportation Systems*, vol. 21, no. 3, pp. 1054–1063, 2020.
- [48] B. Tian, G. Wang, Z. Xu, Y. Zhang, and X. Zhao, "Communication delay compensation for string stability of cacc system using lstm prediction," *Vehicular Communications*, vol. 29, Article ID 100333, 2021.
- [49] X. Zhu, Y. Shen, Z. Zhang, and M. Yan, "Stability analysis of the vehicular platoon with sensing delay and communication delay: CTCR paradigm via dixon resultant," *Applied Sciences*, vol. 13, Article ID 11807, 2023.
- [50] J. Lai, J. Hu, L. Cui, Z. Chen, and X. Yang, "A generic simulation platform for cooperative adaptive cruise control under partially connected and automated environment," *Transportation Research Part C: Emerging Technologies*, vol. 121, Article ID 102874, 2020.